applied sciences

MDPI

Article

Synthesis of Zeolitic Material with High Cation Exchange Capacity from Paper Sludge Ash Using EDTA

Takaaki Wajima

Department of Urban Environment Systems, Graduate School of Engineering, Chiba University, 1-33, Yayoi-cho, Inage-ku, Chiba 263-8522, Japan; wajima@tu.chiba-u.ac.jp; Tel.: +81-43-290-3507

Abstract: Paper sludge ash (PSA) typically has a low Si abundance and significant Ca content because of the presence of calcite fillers, which interfere with the zeolitic conversion of PSA. Ca-masking with ethylenediaminetetraacetic acid (EDTA) was used to reduce Ca interference during zeolite synthesis so that a zeolitic product with a high cation exchange capacity (CEC) could be synthesized. Hydroxysodalite, zeolite-P, hydroxycancrinite, tobermorite, and zeolite-A can be synthesized from PSA by an alkali reaction with EDTA. With the addition of EDTA, calcium ions in the solution were trapped by chelation, and the number of zeolitic crystals with low Si/Al (Si/Al = 1), zeolite-A, increased owing to the promotion of the synthesis reaction. A product with a high CEC that has a high zeolite-A content was obtained. The chelating agent can inhibit Ca interference for zeolite synthesis by Ca-masking, and a product with a high zeolite-A content can be obtained from PSA using EDTA.

Keywords: paper sludge ash; EDTA; zeolite-A; cation exchange capacity; Ca-masking

Citation: Wajima, T. Synthesis of Zeolitic Material with High Cation Exchange Capacity from Paper Sludge Ash Using EDTA. *Appl. Sci.* **2021**, *11*, 11231. https://doi.org/10.3390/app112311231

Academic Editor: Nikolaos Koukouzas

Received: 13 October 2021
Accepted: 25 November 2021
Published: 26 November 2021

1. Introduction

Zeolites are a group of microporous aluminosilicate minerals that are tectosilicates with three-dimensional aluminosilicate structures containing water molecules, alkali, and alkaline earth metals in their structural framework [1,2]. Zeolites have unique properties owing to their specific structure, i.e., their aluminosilicate skeleton structure with a hierarchical character. The center of the tetrahedron is an atom "T" (Si or Al), which is linked to four other T-atoms by an oxygen bond. The tetrahedrons AlO_4 and SiO_4 are known as the primary building units (PBUs). These tetrahedrons can be arranged into larger structures called secondary building units (SBUs) consisting of up to 16 T atoms, and it is assumed that the entire framework is made up of only one type of SBU. Presently, 23 different types of SBUs are known to exist, and approximately 250 zeolite framework types have been defined in the "Atlas of zeolite framework types" [3].

Based on the Si/Al ratio, zeolites can be divided into: (i) low (1–1.5), (ii) intermediate (2–5), (iii) high silica zeolites (10–100), and (iv) silica molecular sieves (>100) [4]. With decreasing Si/Al ratios, the zeolites are more hydrophilic and have a greater affinity for polar adsorbates. Generally, according to Loewenstein's role, the amount of tetrahedral AlO_4 should not be higher than SiO_4 in the zeolite structure, and the lowest Si/Al ratio has the highest negative charge in the skeleton structure [5].

Zeolites occur naturally in the environment, but they can also be synthesized in a laboratory or industry [6]. The outstanding physicochemical properties of zeolites, such as their cation exchange, catalysis, and sorption, make them very useful in a variety of industrial [7,8], environmental [9–11], biotechnological [12–14], biomedical [15,16], and medical applications [17,18]. Numerous researchers have reported the synthesis of various types of zeolites (such as zeolite-A, P, and X, and ZSM-5) from industrial waste (for example, coal fly ash, paper sludge ash, municipal incinerated ash, and waste porcelain or perlite), which are mainly composed of SiO_2 and Al_2O_3 in amorphous phases [19–27], via different

hydrothermal activation methods, such as classic alkali activation [28], alkali fusion [29], two-stage synthesis [30], acid leaching [31], and addition of silica sources [32,33].

In the manufacture of recycled paper, paper sludge is discharged as industrial waste, and its amounts have continued to increase annually worldwide, for example, 11 million tons were discharged in Europe [34], 5.1 million tons were generated in Japan [35], and 2.6 million tons were generated in Korea [36]. Paper sludge ash (PSA) is produced by the fluidized bed combustion of paper sludge for the volume reduction of waste sludge for landfills (80–90% reduction) and partial recovery of energy from paper sludge combustion. Although a part of PSA is used for some applications such as soil improvement, cement additives, and water treatment [37,38], a large part of the ash is landfilled to cause environmental problems, incurring high costs for the paper industry due to the shortage of landfill sites. Therefore, alternative routes to the landfilling and valorization of PSA are desired.

In the past few decades, PSA has been used for the synthesis of functional minerals, such as zeolites and tobermorites [39,40]. Owing to their ion-exchange properties and unique structures, they are used in various applications such as gas removal and water purification [41–43]. Some methods for the chemical conversion of PSA into functional materials exist, such as the conventional hydrothermal reaction [44], alkali fusion [45], and the use of silica additives [46].

Calcite, which is used in this study as a filler, has been recently used to make ash with high calcium content in the form of anorthite, gehlenite, and amorphous phases. Calcium-containing ash can be converted into zeolites, but the product has a low cation exchange capacity (CEC) [47]. In previous studies, we applied acid leaching to reduce the Ca content in calcium-containing ash to synthesize zeolitic materials with high CECs [48–50]. However, in practice, it is difficult to add an acid leaching process before the synthesis process.

In this study, we applied Ca-masking with a chelating agent, ethylenediaminetetraacetic acid (EDTA), to reduce Ca interference during zeolite synthesis. EDTA is the most popular chelating agent and is used as a Ca-masking agent to decrease the hardness of water. Adding EDTA to a conventional reactor is a simple technique that can improve the synthesis of a product with a high CEC. The effect of EDTA on zeolite synthesis from PSA under an alkali reaction was determined to synthesize zeolite materials with a high CEC.

2. Materials and Methods

2.1. Samples

The PSA used in this study was obtained from a major paper manufacturer in Japan. It is noted that the specific surface area of the PSA was 4.5 m^2/g, and it consisted of spherical particles with a diameter of 0.5–2 μm and aggregates with a diameter of 10–100 μm. Ethylenediamine-tetraacetic acid disodium dehydrate (EDTA) (Wako) was used as the chelating agent.

2.2. Experimental Method

To investigate the effect of the addition of EDTA on zeolite synthesis, 10 g of PSA was added to 100 mL of 3 M NaOH solution with an EDTA concentration ranging from 0 to 2 M in a 200 mL Erlenmeyer flask fabricated from polymethylpentene (TPX) and was heated at 80 °C for 24 h in a water bath to synthesize zeolitic material. After heating, the resulting solid was filtered, washed with distilled water, and dried in an oven at 60 °C overnight to obtain the product. The mineralogical composition of the product was identified by X-ray powder diffraction (XRD) (Rigaku, XRD-DSC-XII, Tokyo, Japan) using CuKα radiation (30 kV, 15 mA) over the 2θ range of 5–55° (scan speed of 5°/min and step scan size of 0.02). The morphologies of the products were observed using a scanning electron microscope (SEM) (JEOL, JSM-6510A, Tokyo, Japan) under a vacuum pressure of 1×10^{-6} Pa and an accelerating voltage of 15 kV. The concentrations of Si, Al, and Ca in the filtrate after synthesis were analyzed using inductively coupled plasma spectrometry (ICP) (Shimadzu, ICP-7500, Kyoto, Japan) (RF power: 1150 W; peristaltic pump speed: 50 r/min; auxiliary gas flow rate: 0.5 L/min; atomizer gas flow rate: 0.7 L/min). The CECs of the

product were measured using the method reported by Wajima et al. [51], as follows. The product was immersed in 1 M ammonium acetate solution, and the solution was shaken for 20 min to replace NH_4^+ in exchangeable sites in the product. It was then centrifuged, and the supernatant was removed by decantation. This procedure was repeated three times. The sample was then washed with 80% EtOH for subsequent replacement. The NH_4^+ in the product was replaced by K^+ using a 10% KCl solution in a procedure that was repeated three times, and the NH_4^+ content in the supernatant was measured. The CEC was calculated using the following equation:

$$\mathrm{CEC(mmol/g)} = \frac{C_{Am} \cdot V}{w}, \quad (1)$$

where C_{Am} is the NH_4^+ concentration in the supernatant (mmol/L), V is the volume of the supernatant solution (L), and w is the weight of the sample (g).

To investigate the effect of temperature on zeolite synthesis, 1 g of PSA was added to 10 mL of 3 M NaOH solution with or without 1 M EDTA in a 50 mL pressure vessel, and the vessel was heated at 80, 120, and 160 °C for 24 h in an electric furnace. After heating, the vessel was quenched with tap water, and the solid product was filtered, washed with distilled water, and dried overnight in an oven at 60 °C. The mineralogical composition of the product was identified by XRD, and the CEC of the product was measured. The morphologies of the products were observed by SEM. The concentrations of Si, Al, and Ca in the filtrate after synthesis were analyzed using ICP.

The zeolitization processes of PSA with and without EDTA were compared to determine the differences in the reaction processes. PSA (100 g) was added to 1 L of 3 M NaOH solution with or without 1 M EDTA in a 1 L Erlenmeyer flask (made of polymethyl pentene) equipped with a dimroth condenser, and the mixture (slurry) was continuously stirred at 80 °C for 24 h. Five milliliter aliquots of the slurry were removed at varying time intervals to monitor the reaction process. The aliquots were filtered, and the filtrates were analyzed by ICP to determine the concentrations of Si, Al, and Ca during the synthesis reaction. The solid product was washed with distilled water and dried overnight at 60 °C. The products were analyzed by XRD and SEM to identify the zeolite phases, and the CECs of the products were measured. The relative crystallinities (RC) of the zeolitic phases in the products were calculated using the method reported by Machado and Miotto [52] using the following equation:

$$RC(\%) = \frac{\sum Intensity\ of\ XRD\ peaks\ of\ the\ product\ phases}{\sum Intensity\ of\ XRD\ peaks\ of\ standard} \times 100. \quad (2)$$

Hydroxysodalite and zeolite-P were prepared using the procedure reported by Kato et al. [53], and these zeolites and commercial zeolite A (MS-4A, Wako, Kyoto, Japan) were used as standards.

3. Results and Discussion

The chemical and mineralogical compositions of the PSA used in this study are shown in Table 1 and Figure 1, respectively. Ash is mainly composed of CaO (42.6%), SiO_2 (28.1%), and Al_2O_3 (18.5%) in the form of crystalline phases, gehlenite ($Ca_2Al_2SiO_7$), anorthite ($CaAl_2Si_2O_8$), and amorphous phases [54].

Table 1. Chemical compositions of the PSA.

Oxide (wt.%)	PSA	Without 1 M EDTA			With 1 M EDTA		
		80 °C	120 °C	160 °C	80 °C	120 °C	160 °C
SiO_2	28.1	31.2	29.0	28.7	41.3	46.2	45.1
Al_2O_3	18.5	12.1	13.0	13.1	24.2	25.8	24.7
CaO	42.6	46.4	47.3	47.2	19.6	11.7	13.3
MgO	4.0	3.5	3.5	3.9	5.1	5.3	5.1
Fe_2O_3	1.6	1.9	1.9	1.9	2.8	3.0	3.0
TiO_2	2.7	3.0	3.1	3.1	4.5	4.8	4.8
Others	2.5	1.9	2.2	2.1	2.5	3.2	4.0

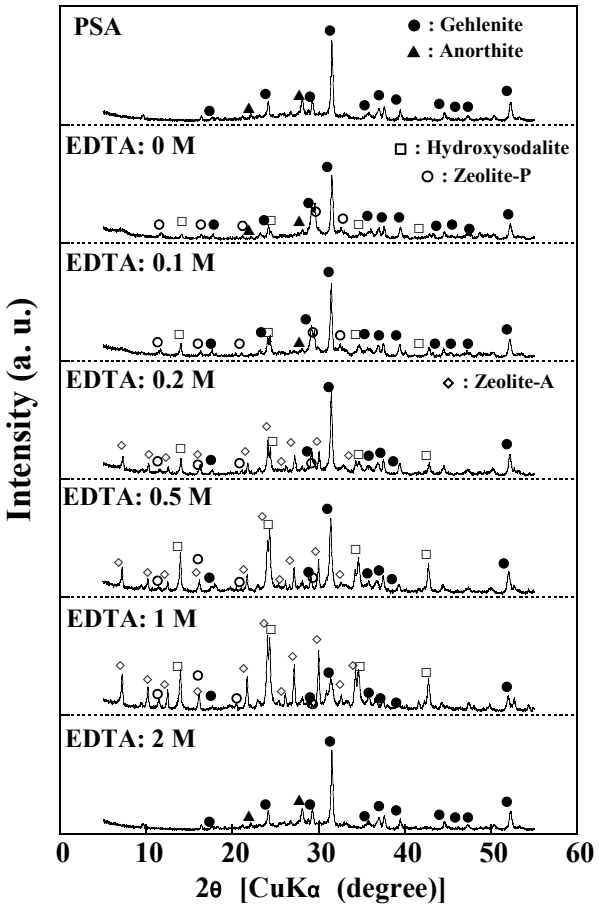

Figure 1. XRD patterns of the products obtained with the addition of EDTA (NaOH concentration: 3 M NaOH, Temperature: 80 °C, Reaction time: 24 h).

Figure 1 also show the XRD patterns of the products as a function of EDTA addition. PSA contains two mineral phases: gehlenite and anorthite. When 1 M EDTA was added, the product phases changed from a mixture of hydroxysodalite ($Na_6Al_6Si_6O_{24}{\cdot}8H_2O$) and zeolite-P ($Na_6Si_{10}Al_6O_{32}{\cdot}12H_2O$) to a mixture of hydroxysodalite, zeolite-P, and zeolite-A ($Na_{12}Si_{12}Al_{12}O_{48}{\cdot}27H_2O$), with high peaks for hydroxysodalite and zeolite-A. For concentrations of EDTA above 1 M, the product had almost the same XRD patterns as raw PSA, indicating that the zeolite synthesis reaction did not occur. Hydroxysodalite is a member of the sodalite group, and its structure comprises a framework of four—and six-membered rings of SiO_4 and AlO_4 tetrahedra. Zeolite-P is a member of the gismondine group, and its structural framework is composed of four- and eight-membered rings. Zeolite-A crystallizes in a typical cubic form, and its structural framework consists of four—and eight-membered rings. Notably, the eight-membered rings are larger than the six-membered rings of hydroxysodalite, while the Si/Al ratio is the same (Si:Al = 1:1). The

order of the Si/Al ratios in the zeolite structure is hydroxysodalite (1:1) = zeolite-A (1:1) < zeolite-P (5:3), and the CEC of zeolite-A is generally higher than those zeolite-P and hydroxysodalite because zeolite-A has a lower Si/Al ratio and ring size.

Figure 2 show the concentration of Si, Al, and Ca in the solution after synthesis as a function of EDTA addition. As the concentration of the added EDTA increased to 1 M, the Ca concentration increased due to Ca-masking with EDTA, and above an EDTA concentration of 1 M, the Ca concentration drastically decreased to zero. The Si concentration increased in the solution with 0–0.3 M EDTA and gradually decreased in the solution with an EDTA concentration higher than 0.3 M. The Al concentration drastically decreased in the solution with 0–0.3 M EDTA and gradually decreased in the solution with an EDTA concentration higher than 0.3 M. Without EDTA addition, the Si, Al, and Ca concentrations in the solution were 227, 2225, and 0 mg/L, respectively, while those in the solution containing 1 M EDTA were 728, 228, and 21,434 mg/L, respectively. Although the reaction between Ca and Si is stronger than that between Si and Al, the Si-Al reaction is promoted by Ca-masking with EDTA [47].

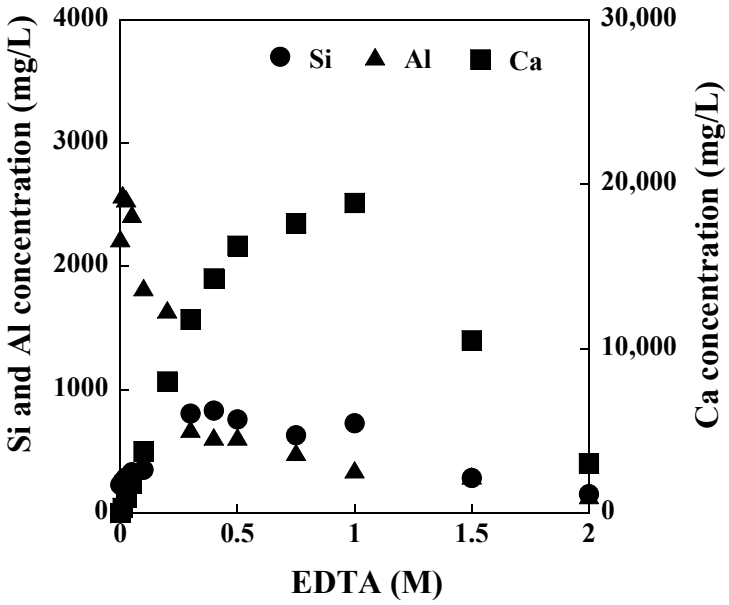

Figure 2. Concentrations of Si, Al, and Ca in the solution after synthesis with various concentrations of added EDTA (NaOH concentration: 3 M NaOH, Temperature: 80 °C, Reaction time: 24 h).

Figure 3 show the relative crystallinities of the zeolite crystals in the product and the CECs of the product as a function of the concentration of the added EDTA. As the concentration of the added EDTA increased to 1 M, the zeolitic phases in the product increased, and the CECs of the product increased from 1.2 to 3.4 mmol/g. The behavior of the CEC as the concentration of EDTA increased is associated with that of the zeolitic phase in the product because Ca masking promoted the reaction between Si and Al to synthesize zeolite crystals, which have a high CEC. These results also indicate that Ca remained in the solution after synthesis owing to Ca-masking by EDTA. Above an EDTA concentration of 1M, the zeolitic phases decreased, and the CECs of the products decreased due to the decrease in Ca-masking in the solution. These results suggest that a product with a high CEC can be synthesized in a 3 M NaOH solution containing 1 M EDTA.

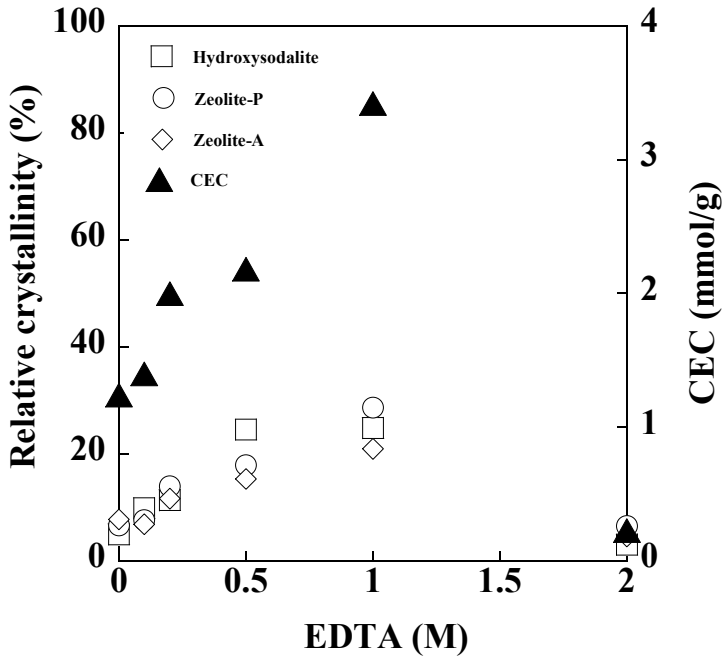

Figure 3. Relative crystalinities of hydroxysodalite, zeolite-P, and zeolite-A in the product, and CECs of the product after synthesis with various concentrations of added EDTA (NaOH concentration: 3 M NaOH, Temperature: 80 °C, Reaction time: 24 h).

The XRD patterns of PSA and the products synthesized from raw ash at various temperatures after a 24-h of reaction with or without 1 M EDTA are shown in Figure 4. PSA contains two mineral phases: gehlenite and anorthite. For the product synthesized without 1 M EDTA (Figure 4a), the anorthite peaks are less intense than those in the raw ash, indicating that a part of the anorthite dissolves in the alkali solution, whereas gehlenite does not seem to be affected at 80 °C. The phases formed were hydroxysodalite and zeolite-P. At 120 °C, anorthite was absent from the products, indicating that most of it dissolved in the alkali solution, while the gehlenite peaks were less intense than those in raw ash and the product at 80 °C, indicating that some of the gehlenite dissolved in the alkali solution. The phases formed were hydroxysodalite and zeolite-P. At 160 °C, both anorthite and gehlenite were absent, indicating that most of them dissolved in the alkali solution. The phases formed were tobermorite ($Ca_5(HSi_3O_9)_2 \cdot 2H_2O$) and hydroxycancrinite ($Na_8(OH)_2Al_6Si_6O_{24} \cdot 2H_2O$) because the increase in Ca supply from gehlenite and the high temperature caused a change in the crystal phases of the product [1,40,55]. It should be noted that the CEC of hydroxycancrinite is generally lower than that of zeolite-A, even though it is Si/Al = 1. In the case of the product obtained in a solution containing 1 M EDTA (Figure 4b), the anorthite peaks are less intense than those in the raw ash, indicating that a part of the anorthite dissolved in the alkali solution, whereas gehlenite did not seem to be affected at 80 °C. The phases formed were hydroxysodalite, zeolite-P, and zeolite-A. At 120 °C, anorthite was absent from the products, indicating that most of it dissolved in the alkali solution, whereas the gehlenite peaks were less intense than those in raw ash and the product at 80 °C, indicating that some of the gehlenite dissolved in the alkali solution. At 160 °C, both anorthite and gehlenite were absent, indicating that most of them dissolved in the alkali solution. The phases formed at 120 °C and 160 °C were hydroxysodalite and hydroxycancrinite, respectively. Although the dissolution behaviors of the mineral phases, gehelenite and anorthite, in raw ash are almost the same, the product phases differ with EDTA addition. It should be noted that the XRD patterns of the products synthesized at 80 °C without EDTA in Figures 1 and 5 are almost the same regardless of stirring or standing.

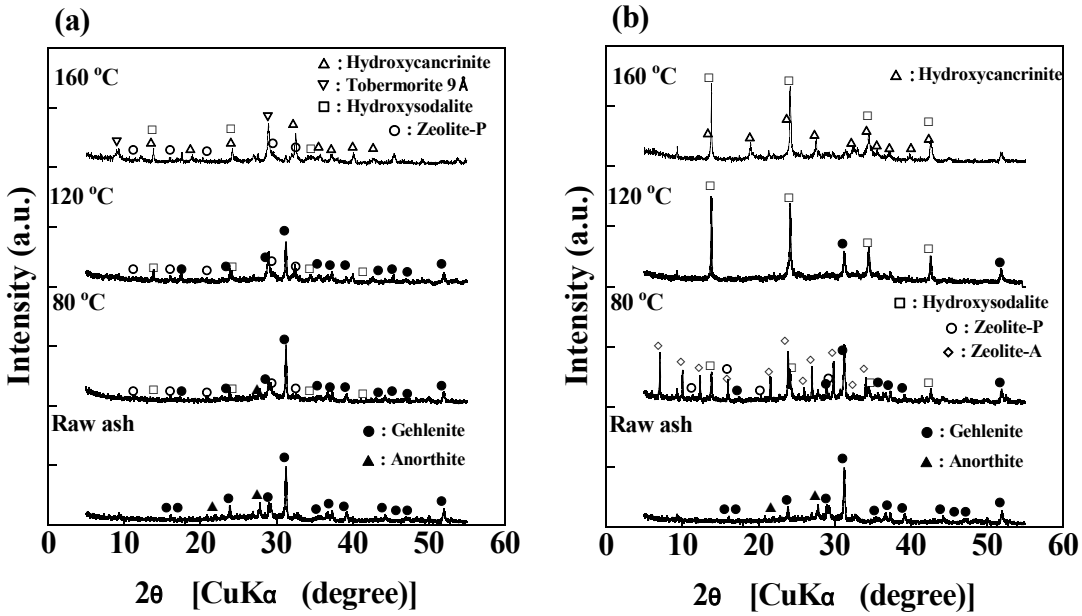

Figure 4. XRD patterns of the products synthesized at 80, 120, and 160 °C: (**a**) without 1 M EDTA and (**b**) with 1 M EDTA (NaOH concentration: 3 M NaOH, Reaction time: 24 h).

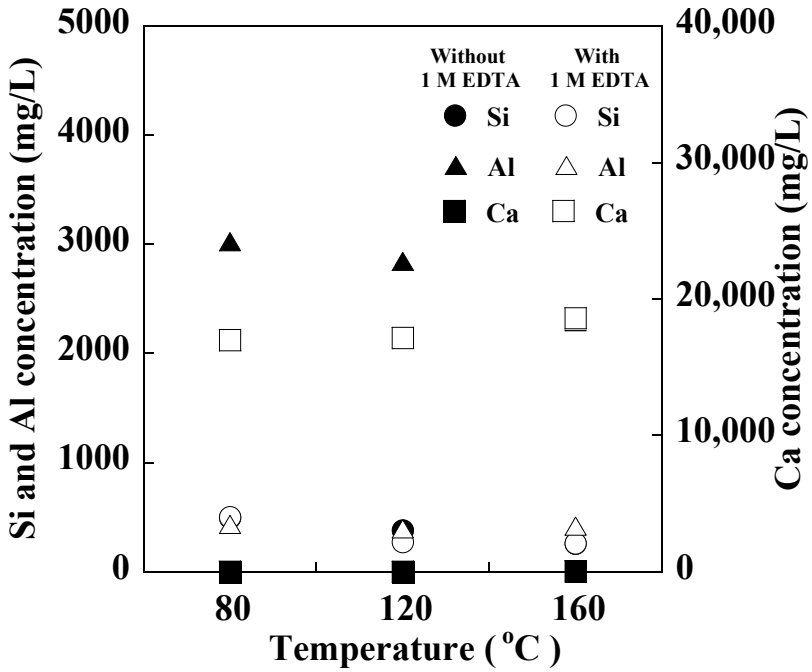

Figure 5. Concentrations of Si, Al, and Ca in the solutions after synthesis at 80, 120, and 160 °C (NaOH concentration: 3 M NaOH, Reaction time: 24 h).

The crystallite sizes (D) of hydroxysodalite, hydroxycancrinite, tobermorite, and zeolite-A in the product were calculated using the Scherrer equation:

$$\mathrm{D\ (nm)} = \frac{K \cdot \lambda}{\beta \cos \theta}, \tag{3}$$

where K is the Scherrer constant, λ is the wavelength of the X-ray radiation, β is the full width at half maximum (FWHM) of the XRD diffraction peaks, and θ is the diffraction angle according to the Bragg formula [56–58]. It is noted that the separation of the peaks for zeolite-P made it difficult to calculate the crystal size. For the products synthesized without

1 M EDTA at 80, 120 and 160 °C, the crystal sizes of hydroxysodalite in the products were 58.0, 57.6 and 50.4 nm, respectively, and those of tobermorite and hydroxycanclinite in the product synthesized at 160 °C were 9.8 and 49.8 nm, respectively. For the products synthesized with 1 M EDTA at 80, 120, and 160 °C, the crystal sizes of hydroxysodalite in the products were 67.3 nm, regardless of the temperature, and those of zeolite-A and hydroxycanclinite in the product synthesized at 80 and 160 °C were 80.1 and 28.5 nm, respectively. It should be noted that temperature and EDTA concentration have little effect on the produced hydroxysodalite, independently synthesizing zeolite-A crystals in the product at 80 °C with EDTA addition.

Figure 5 show the concentrations of Si, Al, and Ca in the solution after synthesis at 80, 120, and 160 °C. At all the temperatures, the Si concentrations in the solutions with and without EDTA after synthesis were almost the same. Furthermore, the Al concentrations in the solutions without EDTA were higher than those in the solutions with EDTA, while the Ca concentrations in the solutions with EDTA were higher than those in the solutions without EDTA. These results can be attributed to the promotion of the Si–Al reaction owing to the capture of Ca by EDTA. It is noted that Ca-masking with EDTA occurs similarly at 80–160 °C.

Table 1 show the chemical compositions of the products synthesized from raw ash with or without 1 M EDTA after a 24 h reaction at 80, 120, and 160 °C. Regardless of the temperature, the decrease in the Ca content in the product with 1 M EDTA was greater than that without 1 M EDTA, whereas the increase in the contents of Si and Al in the product with EDTA was greater than that without EDTA. These results were corroborated by the concentrations of Si, Al, and Ca determined after the 24 h reaction (Figure 5), indicating that the Si–Al reaction was promoted with the addition of 1 M EDTA because the remaining Ca in the solution was masked by EDTA.

Figure 6 show the CECs of PSA and the synthesized products with and without 1 M EDTA at various temperatures. The CECs of all the products were higher than that of raw ash (0.3 mmol/g). Regardless of the temperature, the CECs of the products with 1 M EDTA were higher than those of products without 1 M EDTA. With increasing reaction temperature, the CEC of the product with EDTA decreased from 2.3 mmol/g at 80 °C to 1.4 mmol/g at 160 °C, owing to the formation of zeolitic crystal phases with lower CEC, i.e., hydroxysodalite and hydroxycancrinite, instead of zeolite-A and zeolite-P.

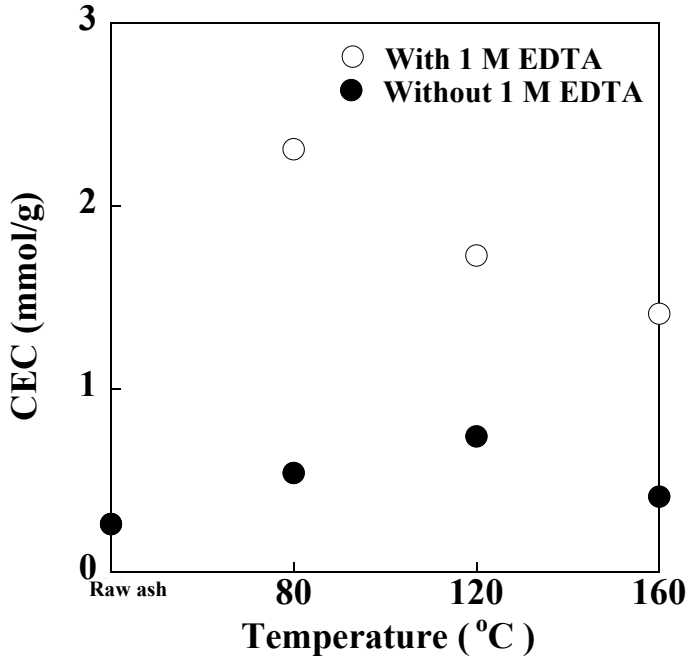

Figure 6. CECs of PSA and the products synthesized from PSA with and without 1 M EDTA at various temperatures (NaOH concentration: 3 M NaOH, Reaction time: 24 h).

Figure 7 show SEM photographs of the products synthesized in solutions with or without 1 M EDTA at 80, 120, and 160 °C. All the products were morphologically different from each other. A higher number of prismatic crystals can be observed in the product synthesized in a solution with 1 M EDTA than in that synthesized in a solution without 1 M EDTA. Platy shape crystals of tobermorite can be observed in the product synthesized at 160 °C without the addition of 1 M EDTA (Figure 7c). Furthermore, cubic crystals of zeolite-A with a size of 1–2 µm can be observed in the product synthesized at 80 °C with EDTA addition (Figure 7d), but these crystals are diminished in the products synthesized at 120 °C and 160 °C with EDTA addition (Figure 7e,f). This is because zeolite-A is a metastable phase at 60–100 °C and is easily transformed into the stable phases hydroxysodalite and hydroxycancrinite at high temperatures [1]. These results suggest, to synthesize a product with zeolite-A phases, which have a high CEC, the reaction temperature should be 80 °C.

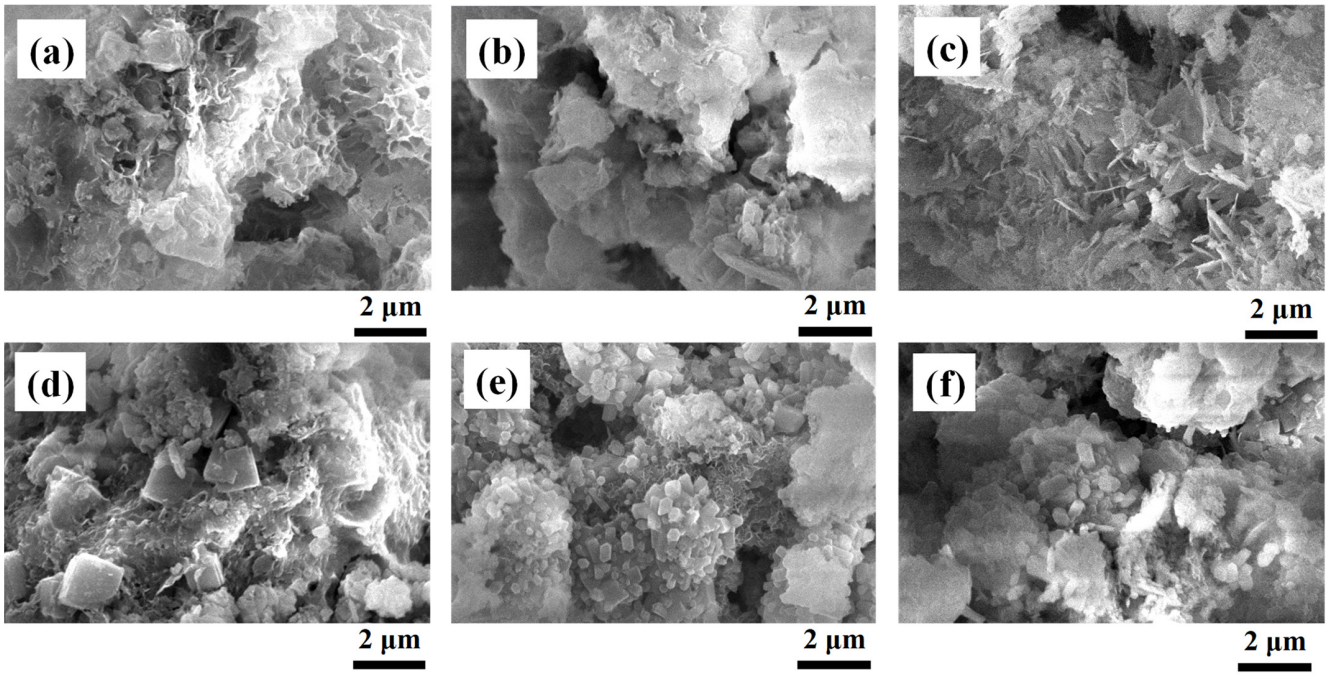

Figure 7. SEM photos of the synthesized products: (**a**) 80 °C without 1 M EDTA, (**b**) 120 °C without 1 M EDTA, (**c**) 160 °C without 1 M EDTA, (**d**) 80 °C with 1 M EDTA, (**e**) 120 °C with 1 M EDTA, and (**f**) 160 °C with 1 M EDTA (NaOH concentration: 3 M NaOH, Reaction time: 24 h).

Figure 8 show the XRD patterns of the products synthesized from raw ash during the reaction at 80 °C with and without 1 M EDTA addition. During synthesis without 1 M EDTA, almost the same patterns were confirmed from 0.5 h to 12 h, and the low peaks of zeolitic product phases (hydroxysodalite and zeolite-P) could be confirmed after the 24 h reaction. In contrast, during the synthesis with 1 M EDTA, almost the same patterns were confirmed from 0.5 h to 4 h, zeolite-A and zeolite-P were confirmed at 6 h, and hydroxysodalite appeared after the 8 h reaction.

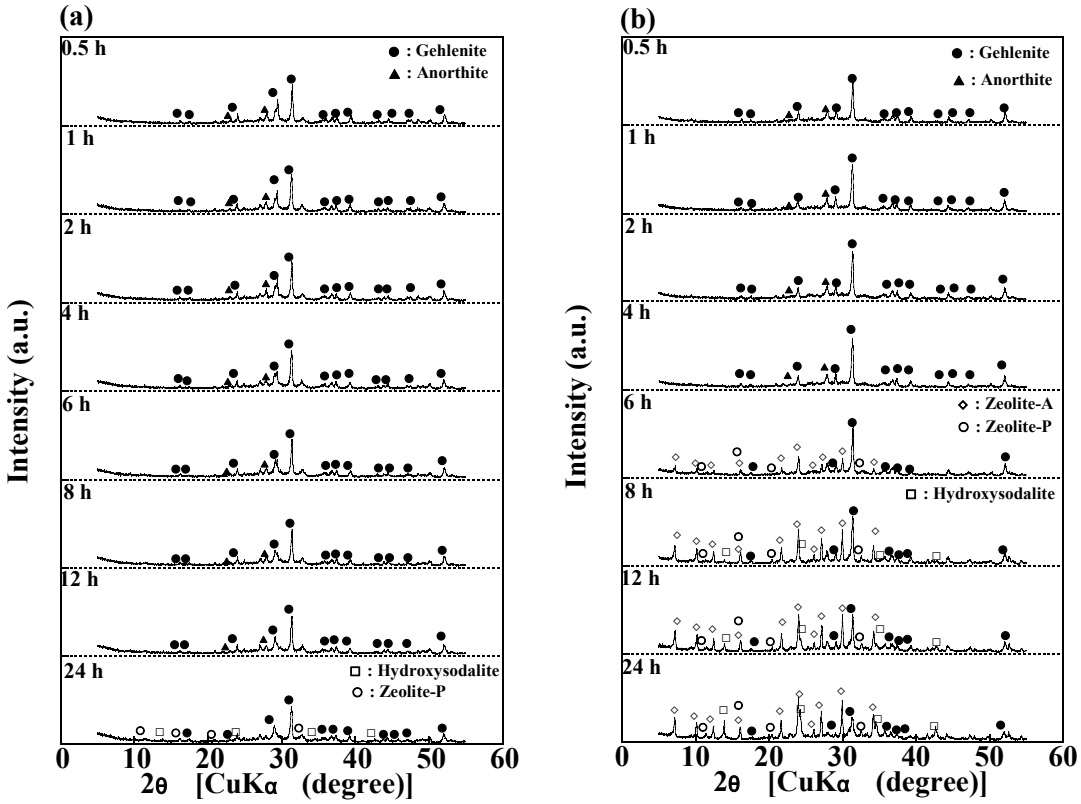

Figure 8. XRD patterns of the products synthesized at 80 °C (**a**) without the addition of 1 M EDTA and (**b**) with 1 M EDTA during the synthesis reaction (NaOH concentration: 3 M NaOH).

The concentrations of Si, Al, and Ca during synthesis with and without 1 M EDTA are shown in Figure 9, and the relative crystallinities of the product phases and CECs of the product during the reaction are shown in Figure 10. In the case of the reaction without 1 M EDTA, the concentration of soluble Al always exceeded that of Si during the reaction, and the Ca concentration was almost zero. Initially, the concentrations of Si and Al increased upon the addition of PSA; however, as the reaction progressed, the Si concentration gradually decreased owing to the formation of aluminosilicate or calcium aluminosilicate gels [55]. The Al concentration started increasing and remained almost constant after 4 h of the reaction. The relative crystallinities of zeolite-P and hydroxysodalite remained almost constant until 12 h and increased afterwards, while the CEC of the product gradually increased during the reaction because of the formation of silicate gels and zeolite crystals. In the case of the reaction with 1 M EDTA, the concentrations of Si, Al, and Ca initially increased, that of Si gradually decreased, that of Ca increased, and that of Al decreased to zero, reaching a steady-state after 8 h. This residual Al concentration was lower than that in the former case, indicating that a large amount of aluminosilicate precipitated out of the solution. The relative crystallinities of zeolite-A and zeolite-P increased after 6 h, whereas that of hydroxysodalite increased after 8 h. The CEC of the product increased for 8 h and then gradually increased, which is consistent with the relative crystallinities of the zeolite phases.

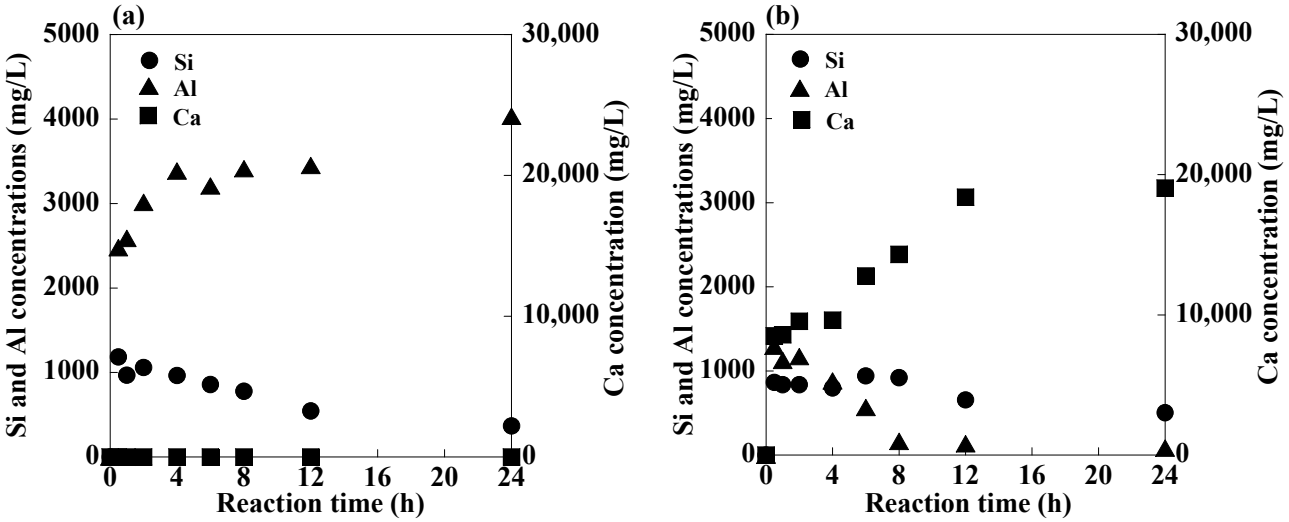

Figure 9. Concentrations of Si, Al, and Ca in the solution during synthesis at 80 °C: (**a**) without 1 M EDTA and (**b**) with 1 M EDTA (NaOH concentration: 3 M NaOH).

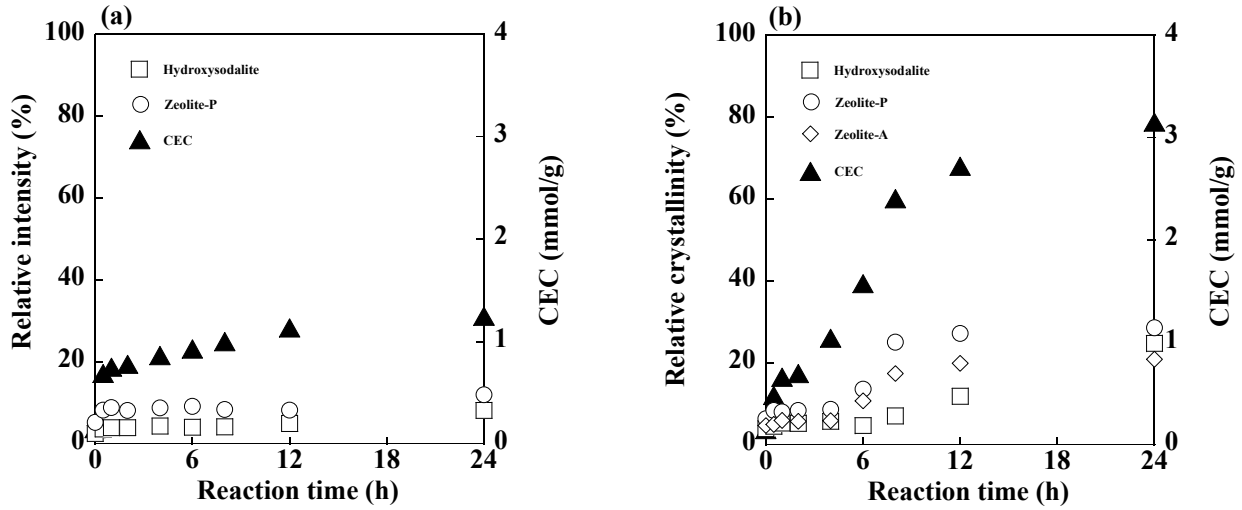

Figure 10. Relative crystallinities of the product phases in the product, and CECs of the product during synthesis at 80 °C: (**a**) without 1 M EDTA and (**b**) with 1 M EDTA (NaOH concentration: 3 M NaOH).

In summary, we propose the following mechanism for 1 M EDTA addition at 80 °C, as shown in Figure 11. Murayama et al. studied the formation of zeolites from coal fly ash and found that zeolite synthesis from coal fly ash consists of three reactions: dissolution, gelation, and crystallization [59]. As shown in Figure 9, the reaction sequence in the present study is consistent with the results reported by Murayama et al. The dissolution, gelation, and crystallization reactions started simultaneously after the ash was introduced. Catalfamo et al. reported that the high affinity of Ca ions for silicate species disturbed the dissolution of Si into the alkali solution [47]. Ando et al. reported that approximately 40% of the Ca content in PSA is present as calcium aluminosilicate hydrate [54]. Without the addition of 1 M EDTA Ca hydrate dissolves into the alkali solution, and the Al content is higher than that of Si because of the Ca interference observed during zeolitization (Figure 9a). The Si, Al, and Ca contents in PSA dissolve into the solution and precipitate as a Si-Al-Ca gel because of the strong reaction between Ca and Si, forming aluminosilicate gels with lower Si/Al ratios in the solid, and the unreacted Si and Al contents remain in the liquid.

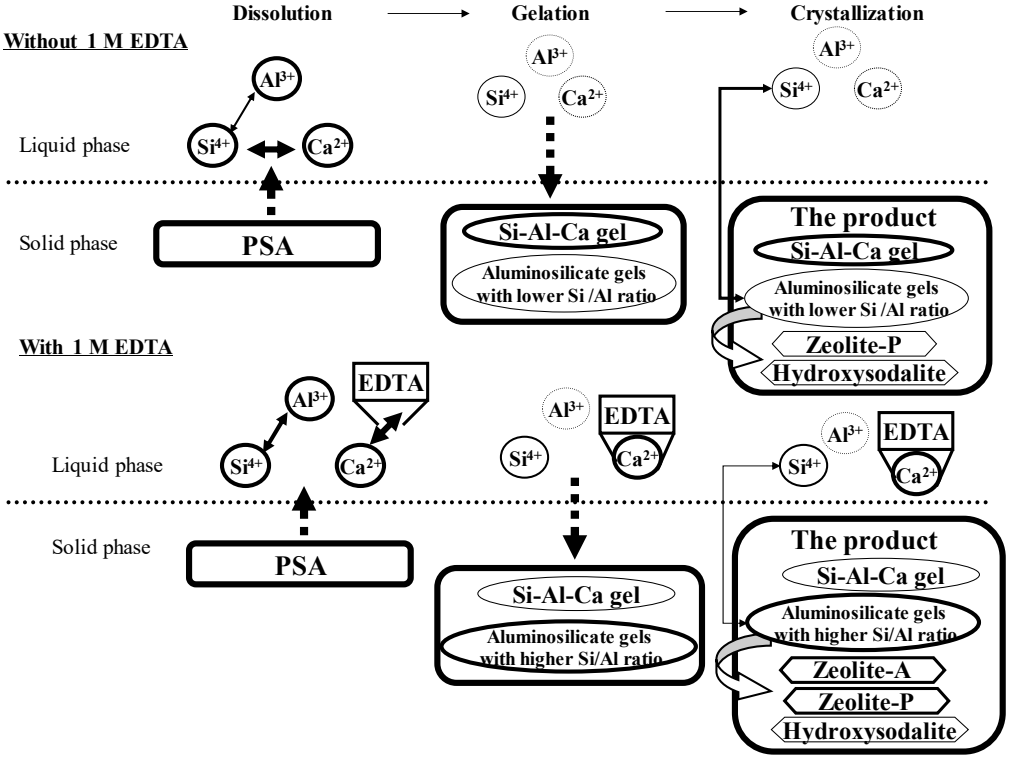

Figure 11. Proposed mechanisms for the zeolitic reaction with the addition of 1 M EDTA at 80 °C.

During the crystallization process at 80 °C, the Si-Al-Ca gel did not react, and the aluminosilicate gels with lower Si/Al ratios reacted with Si in the liquid forming zeolite phases. Therefore, the product synthesized at 80 °C had low hydroxysodalite and zeolite-P contents. With the addition of 1 M EDTA, the Ca hydrate dissolved into the alkali solution, and the concentration of the Al content was almost the same as the Si content because Ca capture by EDTA inhibited Ca interference during zeolitization (Figure 9b). The Si, Al, and Ca contents in PSA dissolved into the solution; the Ca content was masked by EDTA, the aluminosilicate gels with higher Si/Al ratios mainly precipitated, Si and Al remained unreacted, and the Ca content was captured with EDTA in the liquid phase. In the crystallization process, the aluminosilicate gels with higher Si/Al ratios reacted with Si and Al in the liquid phase forming zeolite phases. The interference by Ca content was inhibited by Ca-masking by EDTA, and a high content of the aluminosilicate gels with higher Si/Al ratios were converted into zeolite-A, zeolite-P, and hydroxysodalite.

4. Conclusions

Zeolitic materials with high CEC, including zeolite-A crystals, can be synthesized from PSA with the addition of EDTA because of the inhibition of Ca interference in zeolite synthesis via Ca-masking by EDTA. The following conclusions can be drawn from the results:

(1) EDTA can extract Ca from the solution and inhibit Ca interference during zeolite synthesis by Ca masking.
(2) Hydroxysodalite, zeolite-P, and zeolite-A can be synthesized from PSA using an alkali reaction with EDTA, and the main zeolite phase can be adjusted by the addition of EDTA.
(3) A product with a high CEC, which has a high zeolite-A content, can be obtained.

Therefore, a chelating agent can inhibit Ca interference in zeolite synthesis by Ca-masking, and a product with a high zeolite-A content can be obtained from PSA using an alkali reaction with EDTA.

Funding: This research received no external funding.

Institutional Review Board Statement: Not applicable.

Informed Consent Statement: Not applicable.

Data Availability Statement: Not applicable.

Conflicts of Interest: The author declares no conflict of interest.

References

1. Barrer, R.M. *Zeolites and Clay Minerals as Sorbents and Molecular Sieves*; Academic Press: London, UK, 1978; pp. 1–22.
2. Gottardi, G.; Galli, E. *Natural Zeolites*; Springer: Berlin/Heidelberg, Germany, 1985.
3. McCusker, L.B.; Olson, D.H.; Baerlocher, C. *Atlas of Zeolite Framework Types*; Elsevier: Amsterdam, The Netherlands, 2007. [CrossRef]
4. Kurniawan, T.; Nuryoto, N.; Firdaus, M.A. Zeolite for agriculture intensification and catalyst in Agroindustry. *World Chem. Eng. J.* **2019**, *3*, 14–23.
5. Breck, D.W. *Zeolite Molecular Sieves: Structure, Chemistry and Use*; John Wiley&Sons: New York, NY, USA, 1974.
6. Colella, C.; Mumpton, F.A. *Natural Zeolites for the Third Millennium*; International Committee on Natural Zeolites—ICNZ: Napoli, Italy, 2000.
7. Li, Y.; Li, L.; Yu, J. Applications of zeolites in sustainable chemistry. *Chem* **2017**, *3*, 928–949. [CrossRef]
8. Pan, M.; Zheng, J.; Liu, Y.; Ning, W.; Tian, H.; Li, R. Construction and practical application of a novel zeolite catalyst for hierarchically cracking of heavy oil. *J. Catal.* **2019**, *369*, 72–85. [CrossRef]
9. Adamaref, S.; An, W.; Jarligo, M.O.; Kuznicki, T.; Kuznicki, S.M. Natural clinoptilolite composite membranes on tubular stainless steel supports for water softening. *Water Sci. Technol.* **2014**, *70*, 1412–1418. [CrossRef] [PubMed]
10. Tauanova, Z.; Tsakiridis, P.E.; Mikhalovsky, S.V.; Inglezakis, V.J. Synthetic coal fly ash-derived zeolites doped with silver nanoparticles for mercury (II) removal from water. *J. Environ. Manag.* **2018**, *224*, 164–171. [CrossRef] [PubMed]
11. Li, Z.; Wu, L.; Sun, S.; Gao, J.; Zhang, H.; Zhang, Z.; Wang, Z. Disinfection and removal performance for Escherichia coli, toxic heavy metals and arsenic by wood vinegar- modified zeolite. *Ecotoxicol. Environ. Saf.* **2019**, *174*, 129–136. [CrossRef] [PubMed]
12. Sakaguchi, K.; Matsui, M.; Mizukami, F. Applications of zeolite inorganic composites in biotechnology: Current state and perspectives. *Appl. Microbiol. Biotechnol.* **2005**, *67*, 306–311. [CrossRef]
13. Montalvo, S.; Guerrero, L.; Borja, R.; Sanchez, E.; Milan, Z.; Cortes, I.; De La Rubia, M.A. Application of natural zeolites in anaerobic digestion processes: A review. *Appl. Clay Sci.* **2012**, *58*, 125–133. [CrossRef]
14. Bacakova, L.; Vandrovcova, M.; Kopova, I.; Jirka, I. Applications of zeolites in biotechnology and medicine—A review. *Biomater. Sci.* **2018**, *5*, 974–989. [CrossRef] [PubMed]
15. Hrenovic, J.; Milenkovic, J.; Ivankovic, T.; Rajic, N. Antibacterial activity of heavy metal-loaded natural zeolite. *J. Hazard Mater.* **2012**, *201*, 260–264. [CrossRef]
16. Tavolaro, P.; Catalano, S.; Martino, G.; Tavolaro, A. Zeolite inorganic scaffolds for novel biomedical application: Effect of physicochemical characteristic of zeolite membranes on cell adhesion and viability. *Appl. Surf. Sci.* **2016**, *380*, 135–140. [CrossRef]
17. Stylianou, M.A. Natural zeolites in medicine. In *Handbook of Natural Zeolites*; Inglezakis, V.J., Zorpas, A.A., Eds.; Bentham Science Publishers: Sarja, United Arab Emirates, 2012; pp. 317–334.
18. Kraljevic-Pavelic, S.; Simovic-Medica, J.; Gumbarevic, D.; Filosević, A.; Przulj, N.; Pavelic, K. Critical review on zeolite clinoptilolite safety and medical applications in vivo. *Front. Pharmacol.* **2018**, *9*, 1–15. [CrossRef]
19. Barrer, R.M.; Beaumont, R.; Colella, C. Chemistry of soil minerals. Part XIV. Action of some basic solution on metakaolinite and kaolinite. *J. Chem. Soc. Dalton Trans.* **1974**, *9*, 934–941. [CrossRef]
20. Ruiz, R.; Banco, C.; Pesquera, C.; Gonzalez, F.; Benito, I.; Lopez, J.L. Zeolitization of a bentonite and its application to the removal of ammonium ion from wastewater. *Appl. Clay Sci.* **1997**, *12*, 73–83. [CrossRef]
21. Baccouche, A.; Srasra, E.; Maaoui, M.E. Preparation of Na-P1 and sodalite octahydrate zeolites from interstratified illite-smectite. *Appl. Clay Sci.* **1998**, *13*, 255–273. [CrossRef]
22. Gualtieri, A.F. Synthesis of sodium zeolites from a natural halloysite. *Phys. Chem. Miner.* **2001**, *28*, 719–728. [CrossRef]
23. Boukadir, D.; Bettahar, N.; Derriche, Z. Synthesis of zeolites 4A and HS from natural materials. *Annu. Chim. Sci. Mater.* **2002**, *27*, 1–13. [CrossRef]
24. Querol, X.; Moreno, N.; Umana, J.C.; Alastuey, A.; Hernandez, E. Synthesis of zeolites from coal fly ash: An overview. *Int. J. Coal Geol.* **2002**, *50*, 413–423. [CrossRef]
25. Yang, G.C.C.; Yang, T.-Y. Synthesis of zeolites from municipal incinerator fly ash. *J. Hazard. Mater.* **1998**, *62*, 75–89. [CrossRef]
26. Wajima, T.; Ikegami, Y. Synthesis of zeolitic materials from waste porcelain at low temperature via a two-step alkali conversion. *Ceram. Int.* **2007**, *33*, 1269–1274. [CrossRef]
27. Wajima, T. Synthesis of zeolitic material from green tuff stone cake and its adsorption properties of silver (I) from aqueous solution. *Microporous Mesoporous Mater.* **2016**, *233*, 154–162. [CrossRef]
28. Querol, X.; Umaña, J.C.; Plana, F.; Alastuey, A.; López-Solar, A.; Medinaceli, A.; Valero, A.; Domingo, M.J.; Gracia-Rojo, E. Synthesis of zeolites from fly ash at pilot plant scale. Examples of potential applications. *Fuel* **2001**, *80*, 857–865. [CrossRef]

29. Sigemoto, N.; Hayashi, H.; Miyamura, K. Selective formation of Na-X zeolite from coal fly ash by fusion with sodium hydroxide prior to hydrothermal reaction. *J. Mater. Sci.* **1993**, *28*, 4781–4786. [CrossRef]
30. Hollman, G.G.; Steenbruggen, G.; Janssen-Jurkovicova, M. A two-step process for the synthesis of zeolites from coal fly ash. *Fuel* **1999**, *78*, 1225–1230. [CrossRef]
31. Wajima, T.; Munakata, K. Effect of alkali species on synthesis of K-F zeolitic materials from paper sludge ash for soil amendment. *Chem. Eng. J.* **2012**, *207*, 906–912. [CrossRef]
32. Wajima, T.; Kiguchi, O.; Sugawara, K.; Sugawara, T. Synthesis of zeolite-A using silica from rice husk ash. *J. Chem. Eng. Jpn.* **2009**, *42*, S61–S66. [CrossRef]
33. Wajima, T.; Shimizu, T.; Ikegami, Y. Synthesis of zeolites from paper sludge ash and their ability to simultaneously remove NH_4^+ and PO_4^{3-}. *J. Environ. Sci. Health A* **2007**, *42*, 345–350. [CrossRef]
34. Monte, M.C.; Fuente, E.; Blanco, A.; Negro, C. Waste management from pulp and paper production in the European Union. *Waste Manag.* **2009**, *29*, 293–308. [CrossRef] [PubMed]
35. Kinoshita, N.; Ujike, I.; Kawai, K.; Kawaguchi, T.; Yasuhara, H.; Nagae, T. Performance evaluation of low carbon concrete using paper sludge ash. *J. MMIJ* **2017**, *133*, 132–139. [CrossRef]
36. Jang, H.; Lim, Y.T.; Kang, J.H.; So, S.; So, H. Influence of calcination and cooling conditions on pozzolanic reactivity of paper mill sludge. *Constr. Build. Mater.* **2018**, *166*, 257–270. [CrossRef]
37. Bui, N.K.; Satomi, T.; Takahashi, H. Influence of industrial by-product and waste paper sludge ash on properties of recycles aggregate concrete. *J. Clean. Prod.* **2019**, *214*, 403–418. [CrossRef]
38. Mavroulidou, M. Use of waste paper sludge ash as a calcium-based stabilizer for clay soils. *Waste Manag. Res.* **2018**, *36*, 1066–1072. [CrossRef]
39. Mun, S.P.; Ahn, B.J. Chemical conversion of paper sludge incineration ash into synthetic zeolite. *J. Ind. Eng. Chem.* **2001**, *7*, 292–298.
40. Coleman, N.J.; Brassington, D.S. Synthesis of Al-substituted 11Å tobermorite from newsprint recycling residue: A feasibility study. *Mater. Res. Bull.* **2003**, *38*, 485–497. [CrossRef]
41. Belviso, C. State-of-art applications of fly ash from coal and biomass: A focus on zeolite synthesis processes and issues. *Prog. Energy Combust. Sci.* **2018**, *65*, 109–135. [CrossRef]
42. Koshy, N.; Singh, D.N. Fly ash zeolites for water treatment applications. *J. Environ. Chem. Eng.* **2016**, *4*, 1460–1472. [CrossRef]
43. Lee, C.-H.; Park, S.-W.; Kim, S.-S. Breakthrough analysis of carbon dioxide adsorption on zeolite synthesized from coal fly ash. *Korean J. Chem. Eng.* **2014**, *31*, 179–187. [CrossRef]
44. Wajima, T.; Ishimoto, H.; Kuzawa, K.; Ito, K.; Tamada, O.; Gunter, M.E.; Rakovan, J.F. Material conversion from paper sludge ash in NaOH, KOH, and LiOH solutions. *Am. Mineral.* **2007**, *92*, 1105–1111. [CrossRef]
45. Wajima, T.; Sugawara, K. Material conversion from various incinerated ashes using alkali fusion method. *Int. J. Soc. Mater. Eng. Resour.* **2010**, *17*, 47–52. [CrossRef]
46. Wajima, T.; Shimizu, T.; Ikegami, Y. Zeolite synthesis from paper sludge ash with addition of diatomite. *J. Chem. Technol. Biotechnol.* **2008**, *83*, 921–927. [CrossRef]
47. Catalfamo, P.; Patane, G.; Primerano, P.; Pasquale, S.D.; Corigliano, F. The presence of calcium in the hydrothermal conversion of amorphous aluminosilicates into zeolites: Interference and removal. *Mater. Eng.* **1994**, *5*, 159–173.
48. Wajima, T.; Ikegami, Y. Zeolite synthesis from paper sludge ash via acid leaching. *Chem. Eng. Commun.* **2008**, *195*, 305–315. [CrossRef]
49. Wajima, T.; Munakata, K. Removal of Ca from paper sludge ash by acid leaching and synthesis of high cation exchange capacity zeolite material. *Int. J. Soc. Mater. Eng. Resour.* **2011**, *18*, 7–10. [CrossRef]
50. Wajima, T. Effects of step-wise acid leaching with HCl on synthesis of zeolitic materials from paper sludge ash. *Minerals* **2020**, *10*, 402. [CrossRef]
51. Wajima, T.; Kuzawa, K.; Ishimoto, H.; Tamada, O.; Nishiyama, T. The synthesis of zeolite-P, Linde Type A, and hydroxysodalite zeolites from paper-sludge ash at low temperature (80 °C): Optimal ash-leaching condition for zeolite synthesis. *Am. Mineral.* **2004**, *89*, 1694–1700. [CrossRef]
52. Fernandes Machado, N.R.C.; Malachini Miotto, D.M. Synthesis of Na–A and –X zeolites from oil shale ash. *Fuel* **2005**, *84*, 2289–2294. [CrossRef]
53. Kato, Y.; Kakimoto, K.; Ogawa, H.; Tomai, M.; Sakamoto, E. An application of hydrothermal crystallized coal fly ashes to wastewater treatment. *Kougyo-Yousui* **1986**, *331*, 27–33.
54. Ando, T.; Sakamoto, T.; Sugiyama, O.; Hiyoshi, K.; Matsue, N.; Henmi, T. Adsorption mechanism of Pb on paper sludge ash treated by NaOH hydrothermal reaction. *Clay Sci.* **2004**, *12*, 243–248. [CrossRef]
55. Wajima, T.; Munakata, K. Material conversion from paper sludge ash in NaOH solution to synthesize adsorbent for removal of Pb^{2+}, NH_4^+ and PO_4^{3-} from aqueous solution. *J. Environ. Sci.* **2011**, *23*, 718–724. [CrossRef]
56. Nassar, M.Y.; Abdelrahman, E.A.; Aly, A.A.; Mohamed, T.Y. A facile synthesis of mordenite zeolite nanostructures for efficient bleaching of crude soybean oil and removal of methylene blue dye from aqueous media. *J. Mol. Liq.* **2017**, *248*, 302–313. [CrossRef]
57. Nassar, M.Y.; Abdelrahman, E.A. Hydrothermal tuning of the morphology and crystalline size of zeolite nanostructures for simultaneous adsorption and photocatalytic degradation of methylene blue dye. *J. Mol. Liq.* **2017**, *242*, 364–374. [CrossRef]

58. Abdelrahman, E.A. Synthesis of zeolite nanostructures from waste aluminium cans for efficient removal of malachite green gye from aqueous media. *J. Mol. Liq.* **2018**, *253*, 72–82. [CrossRef]
59. Murayama, N.; Yamamoto, H.; Shibata, J. Mechanism of zeolite synthesis from coal fly ash by alkali hydrothermal reaction. *Int. J. Miner. Process.* **2002**, *64*, 1–17. [CrossRef]